Simulation of two-body relaxation processes in globular clusters

Dynamics of stellar systems

Giovanni Y. Ferron

---

1 Introduction

Two-body relaxation is a very important process in a variety of stellar systems: even though the interactions between stars can be neglected on a dynamical timescale, they play an important role when determining the extended evolution of a stellar system, making it slowly drift away from its initial distribution. In particular, the effects of relaxation in globular clusters can greatly influence the dynamics of their stars. It is then useful to perform simulations to test these effects in order to predict the behaviour of a cluster on a few relaxation timescales, t_{rel}. The goal of this work is to simulate an isolated cluster initially in equilibrium, and to test the effects of two-body relaxation on its evolution in time. The main effects which are predicted to be seen are three:

- **Core collapse:** the dense core of a cluster is hotter than the more diffuse, colder halo. For this reason the interactions between stars tend to transfer energy from the core to the halo, resulting in halo stars diffusing towards the escape velocity. Instead, stars in the inner regions collapse further into the potential well of the cluster, becoming even hotter due to the negative heat capacity of gravity thus continuing the exchange of energy and making the central density increase. In a single-mass, isolated cluster the process of core collapse is relevant over timescales of $\sim 15-16\ t_{rel}$, while the presence of multiple star masses can decrease this timescale down to $\sim 4-5\ t_{rel}$.
- **Evaporation:** high energy stars that experience many encounters may gain enough energy to become unbound from the cluster. Evaporation is a very slow process, taking $\sim 136\ t_{rel}$ for a single-mass cluster to fully evaporate, so very few stars are expected to escape during core collapse and mass segregation.
- **Mass segregation:** systems with different populations of stars seek to establish equipartition of kinetic energy, leading to an exchange of energy between heavier and lighter stars. In a self-gravitating system this means that heavier stars lose kinetic energy and sink deeper into the potential well, while lighter stars tend to instead expand their orbits. Mass segregation is a relatively fast process compared to single-mass core collapse, taking effect on $\sim t_{rel}$.

2 Simulation strategy

To test two-body relaxation I chose to run two simulations of an isolated globular cluster, each starting from a Plummer sphere in equilibrium with $N = 10^4$ particles, with total mass $M_{tot} = 10^4\ M_\odot$ and scale radius $b = 1\ pc$. One of the simulations is composed of only stars with mass $m = 1\ M_\odot$ to test core collapse, while the other has two populations of stars with different masses ($m_2 = 10m_1$) to test mass segregation.

Cluster initialization

Each simulation starts from an initial distribution that is a Plummer sphere in equilibrium, with the following density and potential profiles:

$$\rho(r) = \frac{3M_{tot}}{4\pi b^3}\left(1+\frac{r^2}{b^2}\right)^{-5/2} \qquad , \qquad \Phi(r) = -\frac{GM_{tot}}{\sqrt{r^2+b^2}} \tag{1}$$

The positions of all particles have been generated by inverse transform sampling of their PDF. Considering that the cumulative distributions of the spherical coordinates, P_r, P_θ and P_ϕ are uniformly distributed in the interval $[0,1]$, the coordinates corresponding to each particle can be computed with equations (2a):

$$\begin{cases} r = b\left(P_r^{-2/3} - 1\right)^{-1/2} \\ \theta = \arccos\left(1 - 2P_\theta\right) \\ \phi = 2\pi P_\phi \end{cases} \quad , \qquad P_r(r) = \frac{M(r)}{M_{tot}} \tag{2a}$$

$$p(v) \propto \left(\frac{v}{v_e}\right)^2 \left(1 - \frac{v}{v_e}\right)^{7/2} \quad , \qquad v_e = \sqrt{-2\Phi(r)} \tag{2b}$$

The velocities required to mantain the sphere in equilibrium on a relaxation timescale are instead computed from the polytropic solution of the Lane-Emden equation with polytropic index $n = 5$, using rejection sampling for the velocity magnitude (since its PDF, shown in equation (2b), cannot be inverted analitically) and computing the direction angles as done with the positions. For the double-mass cluster I added a population of masses such that $m_2 = 10m_1$, keeping the total mass M_{tot} the same. The number of heavy stars was set to be 0.01N so that their impact on the initial density profile is not significant. The generated density and potential profiles and velocity distribution are in agreement with the theoretical ones, as seen in figures 1 and 2.

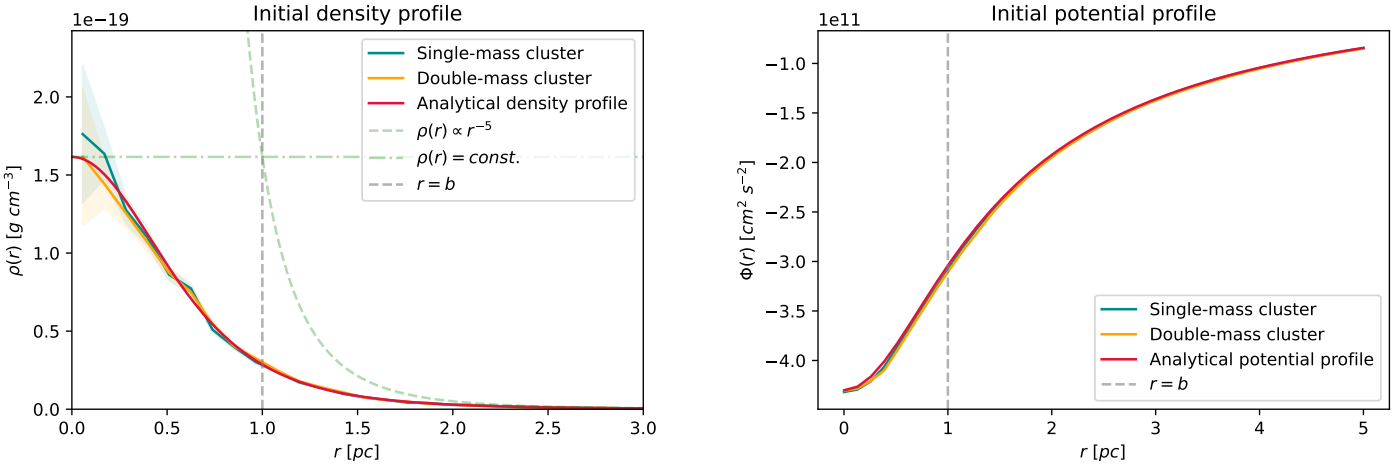

Fig. 1: **On the left (a):** initial density profile for the single-mass and double-mass simulations compared to the theoretical Plummer profile. Both profiles were computed using 45 equally spaced radius bins, extending from $r_{min} = 0$ to $r_{max} = 5b$. The 1σ Poissonian errors are also shown. Both profiles are compatible with the theoretical one. **On the right (b):** initial generated potential profiles and theoretical profile. The generated ones are compatible with the Plummer profile with a relative error of $\sim 0.7\%$ and $\sim 1.25\%$ for the single and double-mass cluster respectively.

Setting simulation parameters

The code I used to run the simulations is the treecode provided by Joshua E. Barnes, as it enables fast force calculations for many more particles than a direct N-body code, but at the cost of some accuracy. The code works in internal units such that $G = 1$, so i chose to set units for distances and masses with $r_{IU} = pc$ and $m_{IU} = M_\odot$. As a result, times and velocities in IU are given by $t_{IU} = 1.5 \times 10^7\ yr$ and $v_{IU} = 6.6 \times 10^3\ cm\ s^{-1}$. The dynamical and relaxation timescales for the Plummer sphere are then approximately equal to:

$$t_{dyn} = \sqrt{\frac{3\pi}{16G\rho_0}} \simeq 0.023\ IU \simeq 3.5 \times 10^5\ yr \tag{3}$$

$$t_{rel} = N_{relax} t_{dyn} \simeq \frac{N}{8 \ln N} t_{dyn} \simeq 3.2\ IU \simeq 4.2 \times 10^7\ yr \tag{4}$$

where ρ_0 is the mean density of the Plummer sphere and N_{relax} is the number of star orbits after which a star velocity is changed significantly from its initial one by encounters. The values of the code parameters have been set the same for both simulations. The softening parameter ε has been chosen considering half of the mean distance between particles:

$$\varepsilon = \frac{1}{2}\left(\frac{\frac{4}{3}\pi R_{median}^3}{N}\right)^{1/3} \simeq 0.04\ IU \tag{5}$$

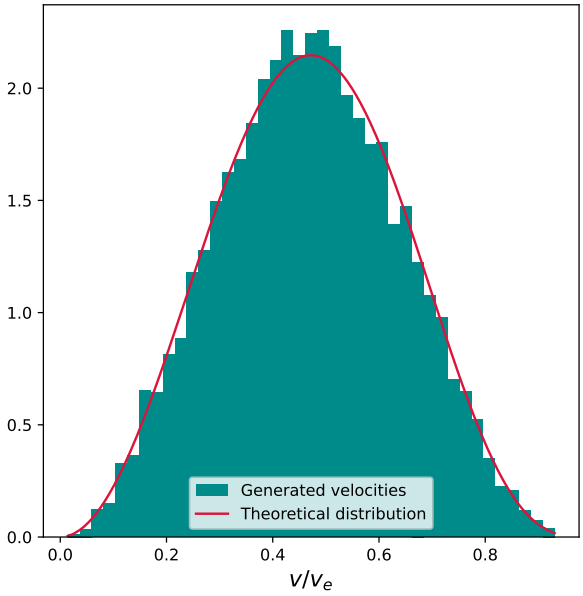

Fig. 2: Generated velocity distribution to mantain the Plummer sphere in equilibrium and theoretical PDF.

Also, the opening angle has been set to $\theta_c = 0.1\ rad$ to have high accuracy. The integration time-step has been set to $dt \sim t_{dyn}/100 \simeq 4 \times 10^{-4}\ IU$. I run the single-mass simulation for $t_{stop} = 44\ IU \simeq 14\ t_{rel}$ based on the core collapse timescale, while the double-mass simulation was run for $t_{stop} = 13\ IU \simeq 4\ t_{rel}$, since the mass segregation timescale is shorter.

3 Results

Single-population cluster

The single-mass simulation is intended to test core collapse. As shown by figure 3a, the total energy stays constant during the evolution of the system with a relative error of 0.33% with respect to the initial value. To check for the formation of a dense core I plotted the density and potential profiles over time: as can be seen in figure 4 there is a significant increase in density and decrease in potential at small radii due to core collapse. There is also a decrease in density and increase in potential at larger radii due to the expansion of the halo.

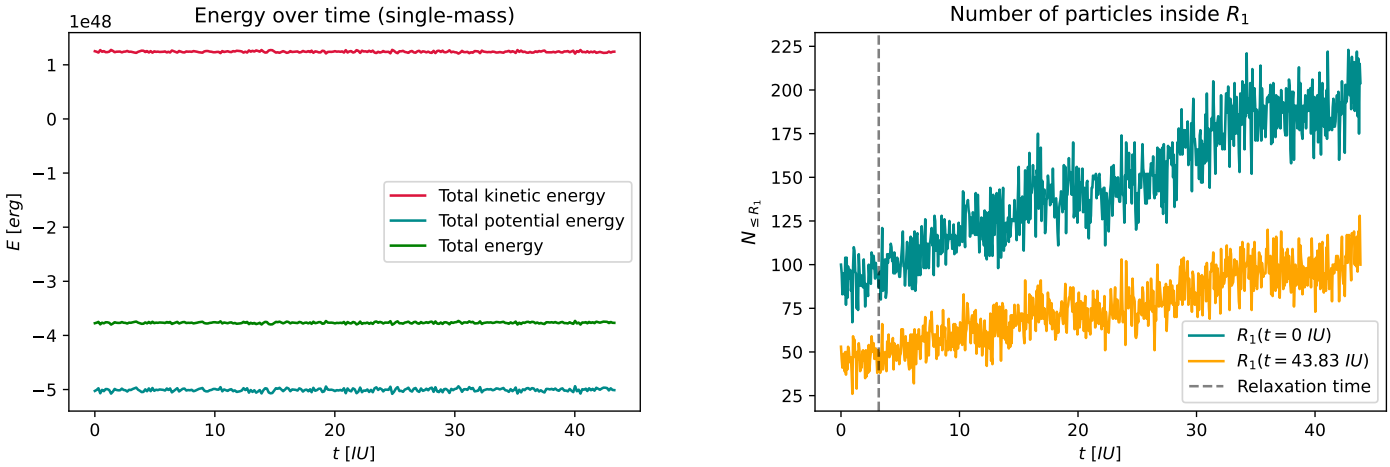

Fig. 3: **On the left (a):** conservation of energy of the single-mass cluster. **On the right (b):** particles inside the 1% Lagrangian radius computed at initial and final time, over the time evolution of the cluster.

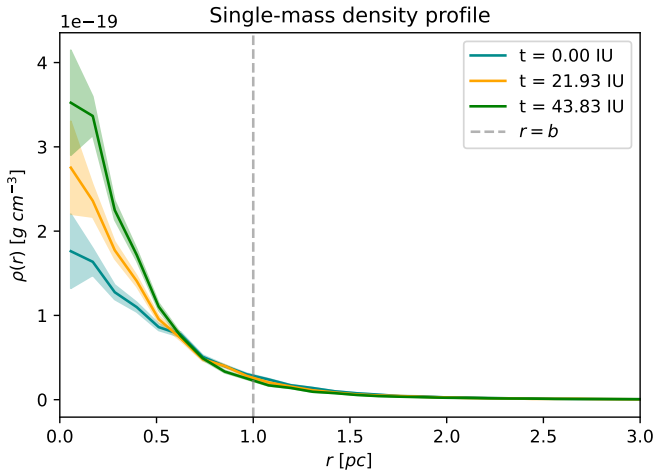

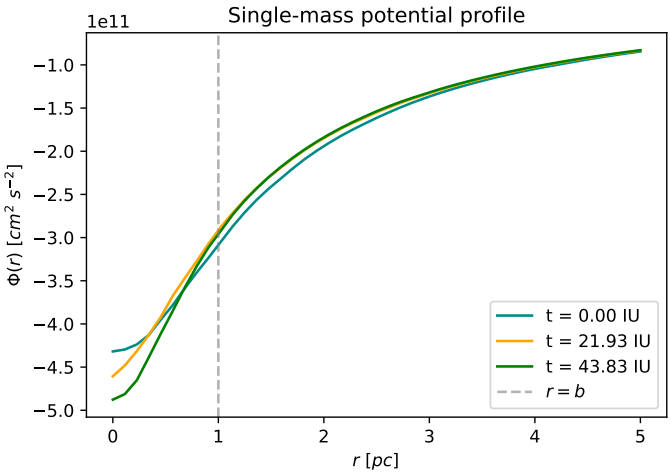

Fig. 4: **On the left (a):** density profiles at different times with Poissonian errors. The central density clearly increases. **On the right (b):** potential profiles at different times. The expansion at larger radii is more visible in the potential profiles than in the density ones.

The formation of a core can also be seen by looking at the Lagrangian radii of the system, shown in figure 5. The radii corresponding to percentages of the total mass smaller than 50% shrink in time as the stars sink deeper towards the center, meanwhile the radii above 50% expand along with the diffusion of the halo. At the end of the simulation each low percentage radius has shrinked by about 24% of their initial value. The half-mass radius R_{50} is instead roughly constant with relative error of $\sim 0.64\%$ with respect to its initial value. Instead, R_{70}, R_{80} and R_{90} expand by about 12%, 19% and 25% respectively. The number of stars inside radii corresponding to R_1 computed at initial and final time also increases confirming that stars are actually collapsing to the center (figure 3b).

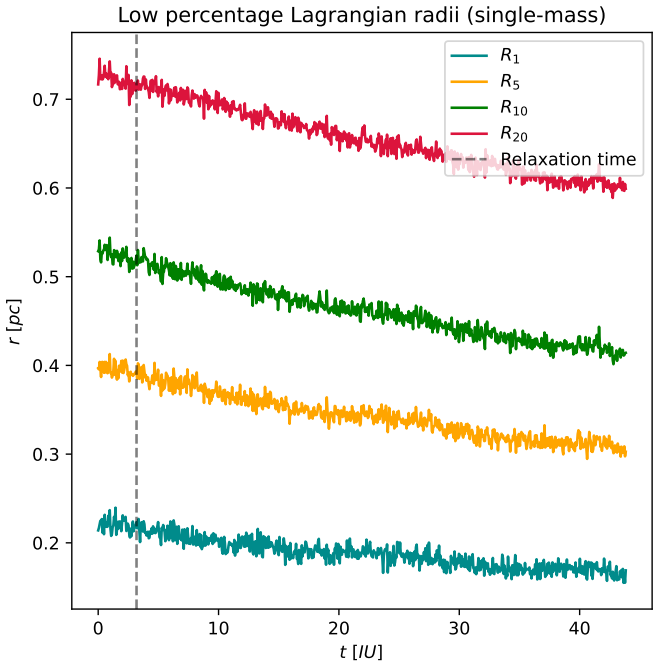

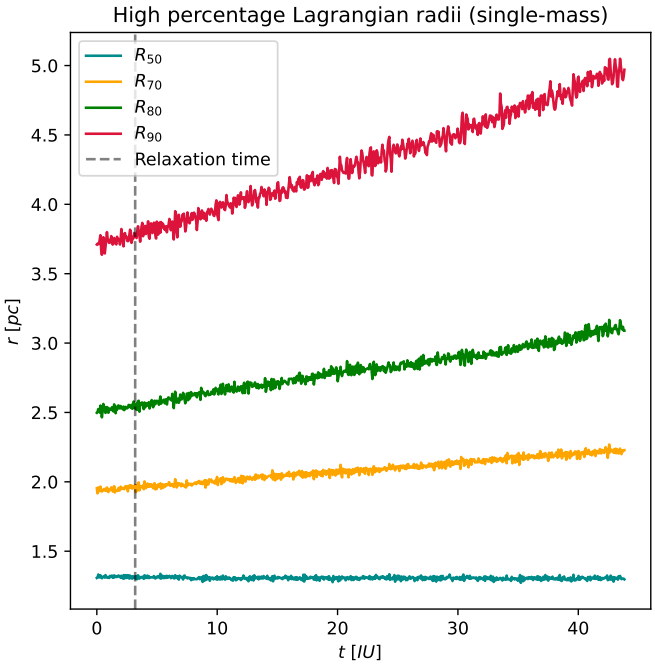

Fig. 5: **On the left (a):** Lagrangian radii for percentages smaller than 50% for the single-mass cluster, clearly decreasing over time. **On the right (b):** Lagrangian radii for percentages equal or bigger than 50%.

During the run the distribution of individual star energies (figure 6a) evolves both towards more negative energies but also to the escape energy. From figure 7 it can be seen that some of the stars that fall to lower energies in figure 6 come from the outer half of the cluster, while some of the stars that gain energy come from the central region. The

halo is then "contaminated" with stars from the inner half, which expand by stealing energy from their companions in the core, making the latter fall deeper into the center. Some stars even manage to become unbound (figure 6b). All these escaped stars originally belong to the halo (outside of R_{50}), their initial orbit is highly elliptical and they all escape sligthly after their periastron. This is due to the fact that, when these stars get closer to the core, they are subject to many more interactions than in the outskirts and so their energy exchange is highest when they are at their lowest radius, causing them to reach the escape energy after a final plunge into the cluster center.

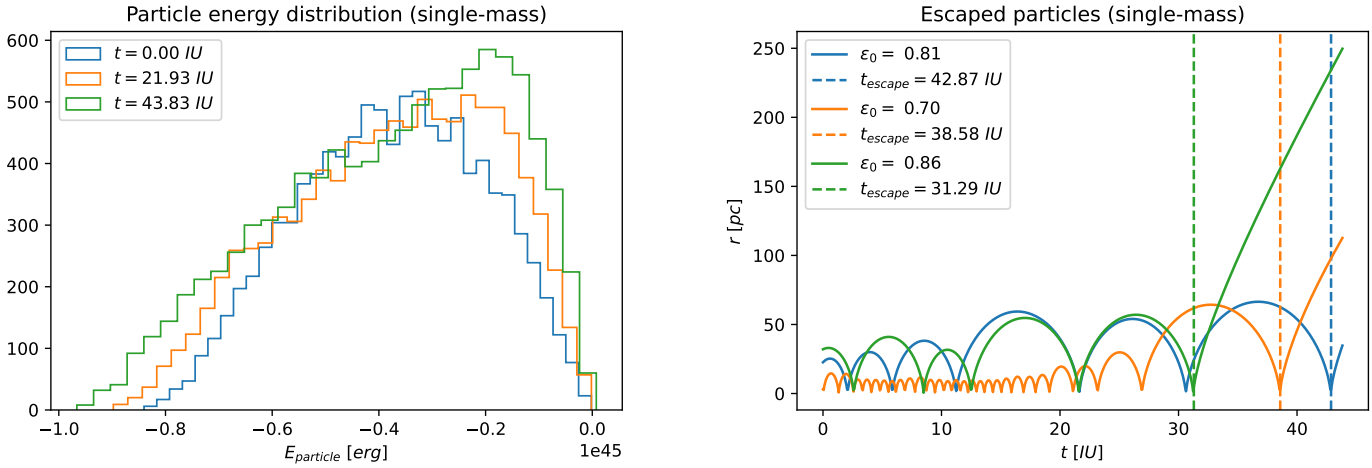

Fig. 6: **On the left (a):** distribution of individual particle energies for the single-mass cluster. **On the right (b):** radii of escaped particles. These particles all have high eccentricity ε_0 and only escape after $t_{escape} \simeq 30\ IU \simeq 9.5\ t_{rel}$. They also have high starting energy, with the more bound one (in orange) having $E_0 = -5.1 \times 10^{43}\ erg$ and starting at radius $r_0 = 3.05\ pc$, way past the half-mass radius $R_{50} \simeq 1.3\ pc$.

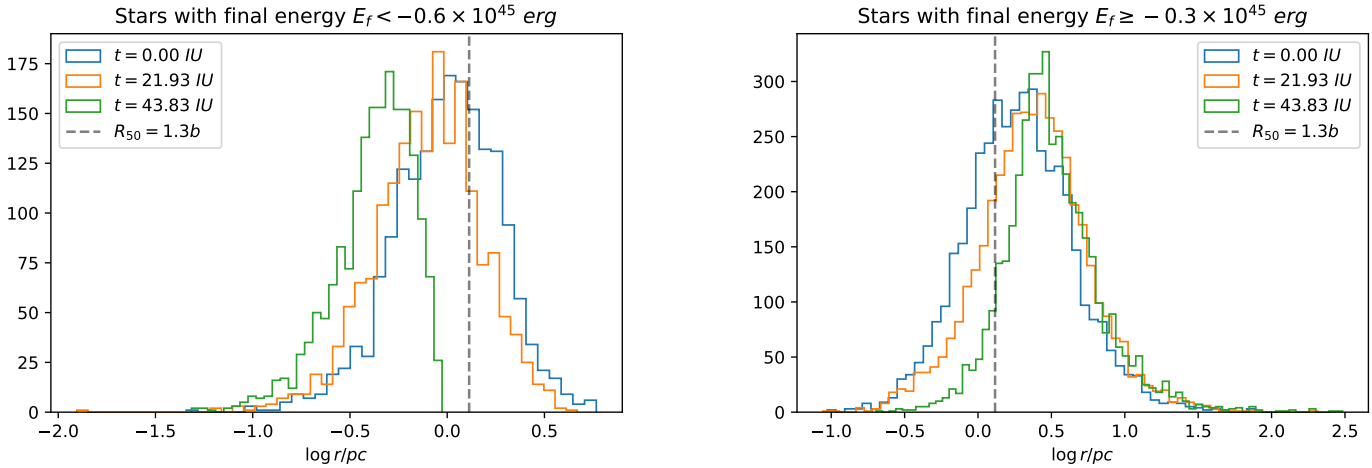

Fig. 7: **On the left (a):** radius distribution of stars which end up with energy at the final time $E_f < -0.6 \times 10^{45}\ erg$. Some of these stars start in the outer half of the cluster, but through unfavourable encounters they lose energy and sink deeper along with the core stars. **On the right (b):** radius distribution of stars with energy at the final time $E_f \geq -0.3 \times 10^{45}\ erg$. As the system evolves some stars from the inner region, with radii below R_{50}, diffuse to higher energy joining the halo stars.

Double-population cluster

In the cluster with two populations of stars mass segregation is evident much earlier than single-mass core collapse. The total energy is still conserved, with a relative error of 0.44% (figure 9). Figure 8 is a top-down view of the cluster, and clearly shows that heavy stars sink deeper into the center over time. The blue and dark blue points represent light and heavy stars respectively, while the red points are heavy stars that are within a scale radius b from the center. In about four relaxation times the fraction of heavy stars inside b is greater than 90%, while more and more light stars expand their orbits.

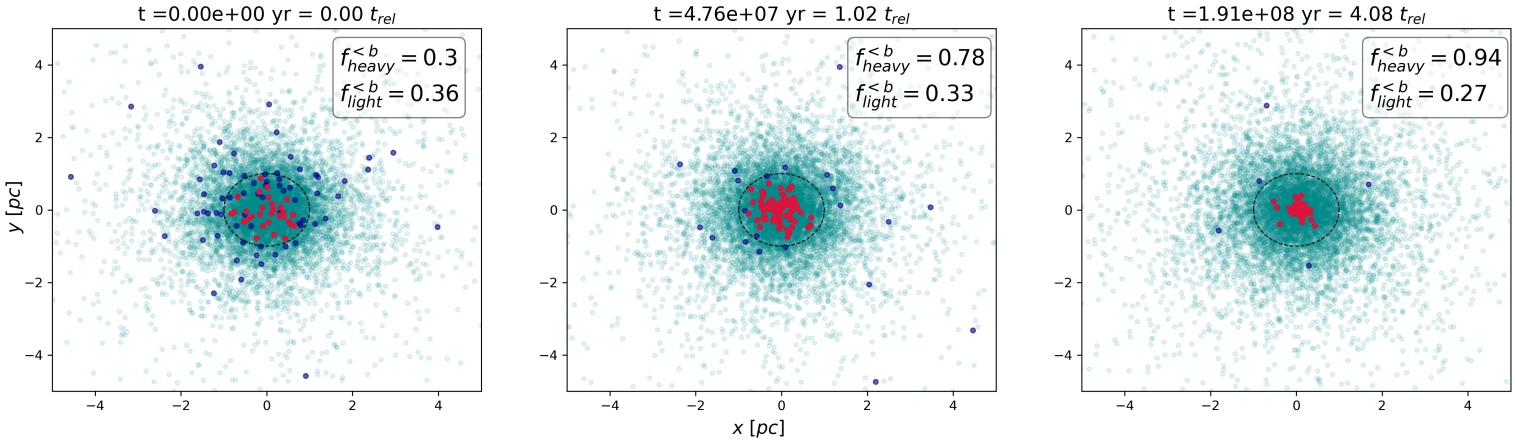

Fig. 8: Projection of the double-mass cluster on the xy plane showing the evolution of the radii of the heavy stars over time, where the dashed line corresponds to $r = b$. The fraction of heavy stars inside a scale radius, denoted $f^{<b}_{heavy}$, is shown to be increasing in time. The fraction of light stars inside b, $f^{<b}_{light}$, is instead decreasing.

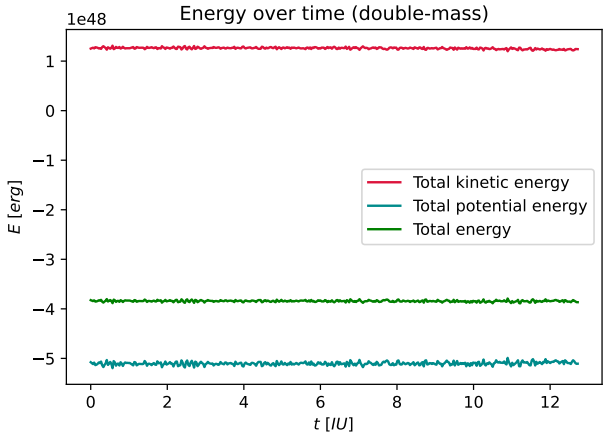

Fig. 9: Conservation of energy of the double-mass cluster.

Mass segregation is also visible in the profiles in figure 10, as the increase in density and decrease in potential is far greater than in the single-mass cluster. The low percentage total Lagrangian radii also shrink faster: the radii R_1 and R_5 have contracted by $\sim 60\%$ at the final time, as seen in figure 11a. The high percentage radii increase due to the expanding orbits of the light stars (figure 11b).

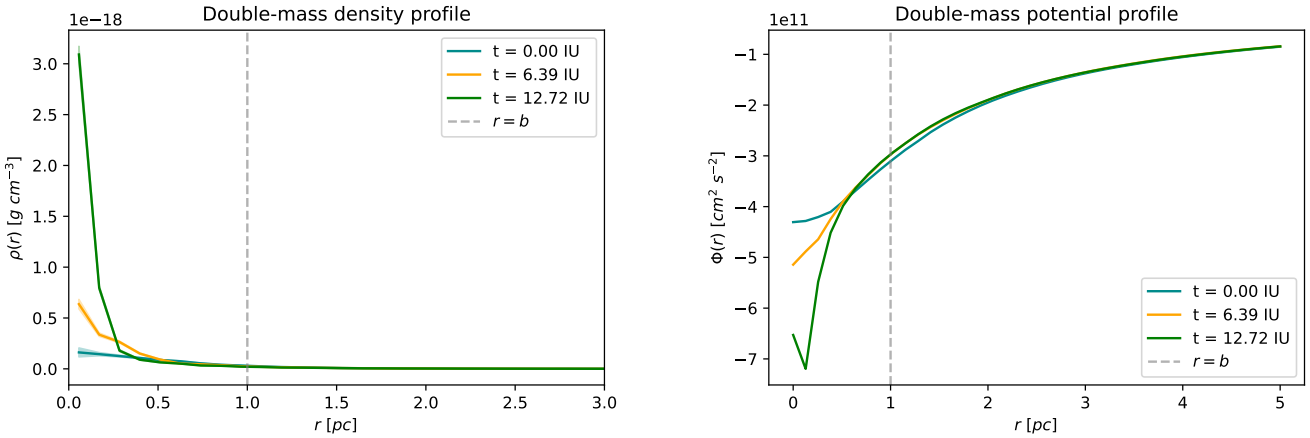

Fig. 10: **On the left (a):** evolution in time of the density profile of the double-mass cluster and Poissonian errors (which are small compared to the values of the density). **On the right (b):** potential profile at different times. In both cases the final profiles show a much greater evolution at lower radii than in the single-mass cluster.

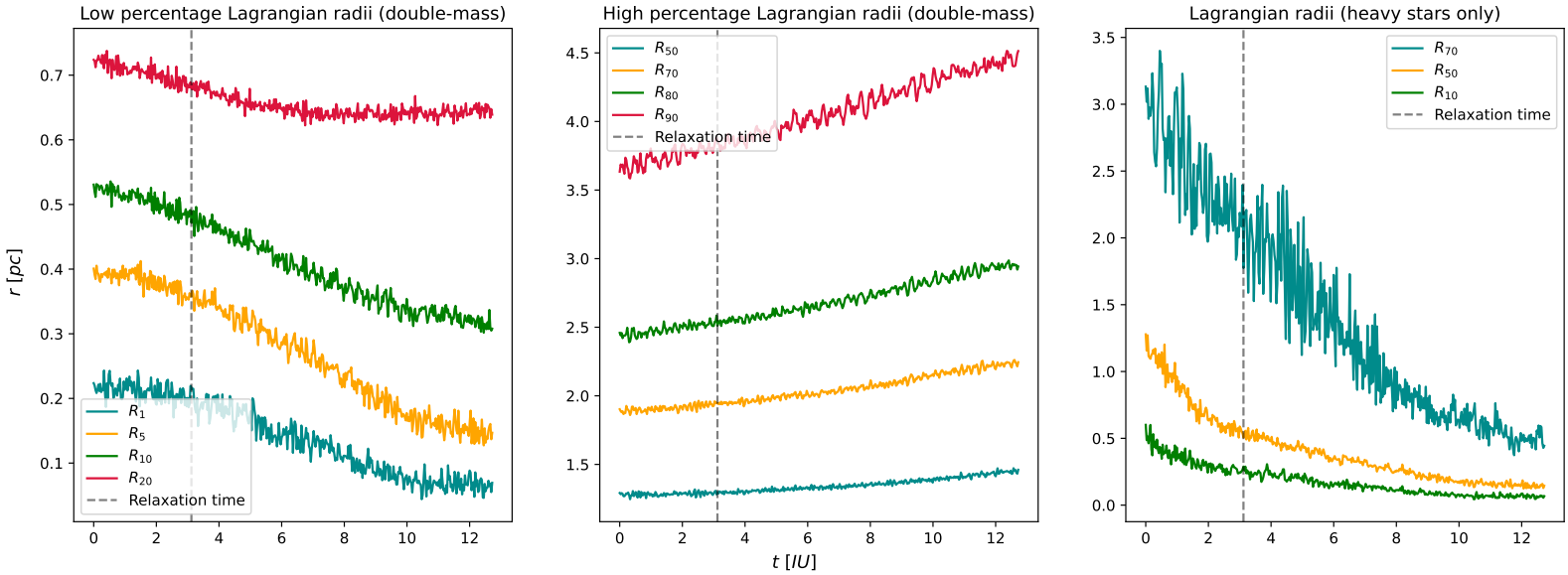

Fig. 11: **On the left (a):** Low percentage Lagrangian radii for the total mass distribution. **In the middle (b):** High percentage total Lagrangian radii. R_{50} is not contant like with the single-mass case. **On the right (c):** Lagrangian radii considering the heavy stars only. For the heavy stars even the high percentage radii contract in time.

The energy distribution in figure 12a is more skewed towards higher energies than the single-mass case. In fact, as shown by figure 12b the few heavy stars all tend to lower and lower energies as they become more bound in the cluster center. Instead, while some light particles collapse (and their energy becomes more negative), the majority of them expand to higher energy (figure 12c). Finally, only one (light) star becomes unbound during the simulation run (figure 12d) but it escapes in a much shorter time than the first escaped star in the single-mass cluster.

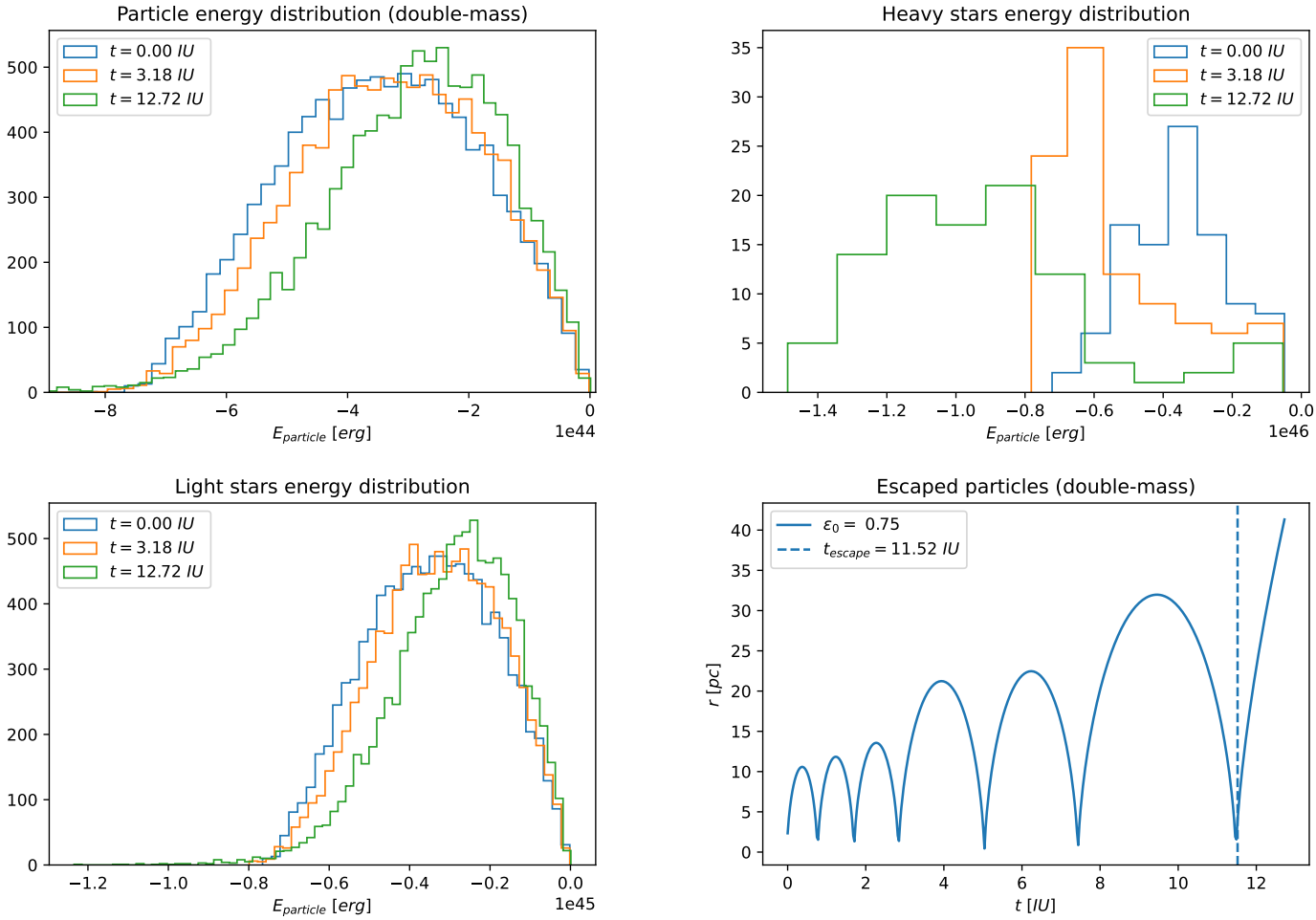

Fig. 12: **Upper left (a):** energy of every particle over time. **Upper right (b):** energy distribution of the heavy stars only. **Lower left (c):** energy distribution of the light stars only. **Lower right (d):** escaped particles. Only one particle manages to be free but it happens sooner than in the single-mass case. Its initial energy is $E_0 = -7.2 \times 10^{43}\ erg$ at radius $r_0 = 2.33\ pc$, so more bound than every escaped star in the single-mass cluster.

4 Conclusions

The focus of this work was testing the effects of relaxation on the evolution in time of globular clusters. In order to do so I ran two simulations of a Plummer sphere in equilibrium, one with a single populations of stars to test core collapse and one with two populations to test mass segregation. From the first simulation I found that the central density increases (and so the potential decreases), a result also confirmed by the shrinking of the low percentage Lagrangian radii. Furthermore, the energy distribution of the particles clearly shows an increase in the number of more bound particles. The second simulation showed a more severe increase in the central density, leading to a greater contraction of the Lagrangian radii. This is indeed caused by an accumulation of heavy stars in the center as predicted. The energy distribution in this case tends more towards less negative energies, due to the large amount of light stars that expand their orbits while the small number of heavy ones collapses. In both simulations some high energy particles managed to escape the cluster. They served to highlight even more differences between the two simulations, such as the fact that, despite being more bound than the single-mass case, the escaped star in the double-mass cluster gained much more energy and so escaped earlier. However, these escaped stars consituted only a very small fraction of the total number, so not a large enough sample to study evaporation in detail.